Numerical Simulation of Flow Past a Square Object Detached with Controlling Object at Various Reynolds Number

Raheela Manzoor[1], Bushra Habib[1], Shazia kalsoom[1], Neelofer Jamil[1], Misbah Haque[2]
[1]Department of Mathematics, Sardar Bahadur Khan Women's University, Quetta, Baluchistan, Pakistan
[2]Department of Management Science, Mir Chakkar Khan University, Sibi, Pakistan
Corresponding Email: raheela_manzoor@yahoo.com

Citation | Manzoor. R, Habib. B, Kalsoom. S, Jamil. N, Haque. M, "Numerical Simulation of Flow Past a Square Object Detached with Controlling Object at Various Reynolds Number", IJIST, Vol. 6 Issue. 2 pp 491-513, May 2024
Received | April 08, 2024, **Revised |** April 15, 2024, **Accepted |** April 18, 2024, **Published |** May 28, 2024.

A two-dimensional (2-D) numerical study has been conducted for flow past of two different configurations of square objects by using the numerical technique Lattice Boltzmann Method (LBM). In these configurations, one object plays the role of the main object, while the second object acts as a controlling object positioned in two different ways, such as firstly placed at the top right corner of the main object (first configuration) and in the second configuration the control object is put at the bottom right corner of the main object at L = 20d (where d is the size of the object). The primary goal of this study was to investigate the impact of the control object on the main object to reduce fluid force and suppress the vortex shedding. Initially, the code's validity was checked, and the effect of the computational domain was studied to determine accurate upstream (L_{up}), and downstream (L_{down}) distances and height of channel (H). Subsequently, all the numerical computations were performed by considering the range of Reynolds numbers ($Re = U_\infty d/\psi$) Re = 80 to 200. The results are presented in terms of vorticity contour, drag (Cd) and lift coefficients (Cl), and physical parameters, including Cd_{mean}, Cd_{rms}, Cl_{rms}, and St. In the vorticity contour, three distinct modes of flow structures were observed for the first configuration (where the control object is placed at the bottom corner of the main object), such as i) Von Karman vortex street (VKVS) flow mode, ii) Two rows vortex street (TRVS) flow mode and iii) Critical flow mode (CF). For the second configuration, two different types of flow modes are identified, dominating the critical flow behavior, those are i) Irregular vortex shedding (IVS) flow mode and ii) Critical flow (CF) mode. The values of Cd_{mean}, Cd_{rms}, Cl_{rms}, and St are calculated against the Reynolds number. For the main object in both configurations, the value of Cd_{mean} decreases at the lower range of Reynolds numbers and then continuously increases at larger values of Reynolds numbers. However, for the control object, the mean drag coefficient consistently increased with an increment in the range of Reynolds numbers. The maximum value of Cd_{mean} is attained at Re = 200, reaching the value of 2.0708 for the configuration where the control object is placed at the top right corner. Similarly, the highest value of the Strouhal number is obtained for the control object; placed at the bottom right corner for C2, with a value of 0.1321 occurring at either Re = 100 or Re = 120.

Keywords: Vortex Shedding, Reynolds numbers, Flow control, Force Statistics, Drag and lift Coefficients.

Introduction:

The complex behavior of fluid flow around objects in various configurations plays a vital role in various fields including ports, shipping, construction, transportation, and engineering. Many experimental and numerical studies available in the literature have explored methods to reduce fluid forces and suppress vortex shedding. These methods include using different arrangements of objects, such as tandem, side-by-side, and staggered configurations, with various shapes like circular, rectangular, square, and triangular. Studying the flow behavior around these objects has enhanced the understanding of fluid dynamics including vortex shedding behavior, pressure distribution, and the forces acting on objects. Some scientists have investigated the object flow during forced oscillations, while others have focused on flow-induced vibrations. The author in [1] conducted a numerical study by considering three distinct object arrangements; inline setting, staggered setting, and side-by-side setting. The author observed that gap spacing (g = s/d) between the objects plays an essential role in determining flow regimes, as it is crucial for creating or reducing fluid forces. The researchers in [2] experimentally studied the vortex shedding frequency and flow interaction among three circular objects arranged in an equidistant triangular cluster at different incidences and gap spacing angles. They found that some well-known flow modes in an array of two objects have been significantly changed in comparison to the presence of a third object.

The researcher in [3] conducted an experimental study for flow past two objects of the same sizes in staggered arrangement at Reynolds number ($Re = U_{inf}\, d/\psi$) ranging from Re = 8500 to 1900. They concluded that vortex shedding frequency was more closely related to the individual shear layer than to the particular object. The researchers in [4] studied the onset of the vortex shedding mechanism for flow past rectangular objects arranged in an in-line and staggered configuration. They concluded that the increment in transverse gap spacing is decreased at the critical Reynolds number for the onset of vortex shedding. The researcher in [5] presented simulations of the staggered configuration at Re = 800, and established five distinct flow modes, that aligned well with existing experimental data, demonstrating consistency in their results. [6] simulated the flow around two side-by-side square objects for different gaps $0.2 \leq g* \leq 6$ and a fixed Reynolds number Re = 150 at a low Mach number ($M = U_\infty/c$), M = 0.2 (therefore, the qualitative features of the flow are not affected by the Mach number). They observed six different flow modes depending on the spacing between objects: non-synchronized, anti-phase, and in-phase synchronized, flip-flopping, single body, and steady modes. The authors in [7], delved into the analysis of gap spacing (g = 0.7d - 2.5d) for flow past two square objects in a staggered arrangement using Lattice Boltzmann Method (LBM) at Re = 73. Their study revealed flip-flopping and synchronized flow patterns, emphasizing the significant influence of gap spacing on these flow regimes. [8] numerically examined the three-dimensional (3-D) flow around two identical square objects arranged in a staggered arrangement at Re = 250 with an incident angle 0^0, highlighting the correlation coefficient between the drag and lift forces, particularly noticeable in the upstream object. [9] investigated the three-dimensional structures behind two circular objects, when they were in tandem arrangement for the range of Reynolds number $160 < Re < 320$.

The author in [10] highlighted the correlation coefficient between the drag and lift forces, particularly in the upstream object. The geometric symmetry in arrangement played a crucial role in discerning flow patterns and vortex-shedding behaviors. [11] conducted numerical simulations using the Lattice Boltzmann Method (LBM) to study liquid flow around two circular objects in a staggered configuration. They observed that the behavior of flow changes at different speeds and angles (θ) ranging from 0^0 to 90^0, at Re = 100. The results are exhibited in terms of streamlines and pressure distribution, illustrating how the different

factors affect the drag and lift forces. [12] experimentally investigated the near wake flow for staggered arrays of short objects by varying the stream-wise gap spacing from 1.73 to 3.46 and Re from 3000 to 4000. It was observed that the Strouhal number (St) is increased by decreasing gap spacing, while the level of turbulent kinetic energy is decreased by increasing gap spacing. In [13], researchers experimentally investigated aerodynamic properties of flow around two circular objects of different sizes at a fixed value of Re = 18900 in a uniform flow field, observing changes in turbulence intensity with object placement in the upstream position. [14] studied the cross-flow past two staggered rows of circular objects at Re = 200, transverse spacing value g = 3, and varying stream-wise gap spacing from g = 0 to 1. They found that stream-wise gap spacing greatly affected the flow regimes and hydrodynamic characteristics of the flow. They also identified high frequencies of shedding vortices for upstream rows of objects. [15] conducted numerical simulation for steady flow past two objects of staggered arrangement by taking the diameter of an object from d = 1.5 to 4 at a low Reynolds number. The direction of cross-flow varies from $\theta = 0^0$ to 90^0. Four distinct vortex-shedding flow modes have been identified. Accurate classification of vortex-shedding regimes around two staggered objects requires combining flow visualization with the analysis of lift forces and velocity signals in the wake.

The researchers in [16] analyzed the dependence of the vortex shedding mechanism and thermodynamic characteristics of flow past two staggered rows of square objects on the dimensionless gap spacing (g^*) at Re = 100. They found chaotic flow behavior at small transverse gap spacings, while traditional vortex dynamics were observed at larger gap spacings. Small stream-wise gap spacing inhibited the vortex shedding process, whereas at large gap spacing regular shedding of vortices persisted. [17] conducted an experimental study on square objects at $Re = 1.3 \times 10^4$, identifying four distinct flow regimes, which included two single-street modes and two double-street modes. Their findings are based on a comprehensive data set that includes Strouhal numbers, flow structures, downstream wake structure mechanism suppression of vortex shedding, etc.

The authors in [18] numerically studied the flow mode and vortex shedding regions for three circular objects in staggered arrangement using the immersed boundary method based on the lattice Boltzmann method. Calculations were conducted at fixed spacing ratios and varying Reynolds numbers ($100 \leq Re \leq 200$). The results indicated that the arrangement significantly influenced the wake structure mechanism and suppression of vortex shedding. [19] conducted a numerical study of flow over two staggered square objects for flow identification. The gap spacing is selected at g = 0.1-6 at Re = 150. By varying the gap ratio, they examined five different flow modes. Furthermore, they noted the maximum drag force experienced by a downstream object, with a maximum Strouhal number observed for an upstream object at g = 1. [20] studied the flow over a square object using an attached control object at Re = 485. They observed the appearance of a secondary vortex at the plate's tail edge after a certain length of the control object, resulting in decreased values of Cdrms and St with increasing control object length. [21] conducted a numerical study on liquid flow around three square objects in a staggered arrangement, varying Re numbers from 1 to 180. In this study, they presented physical constraints including average drag and lift coefficients as well as Strouhal number. They identified two distinct flow modes: steady and unsteady. [22] used the Lattice Boltzmann method to study how fluid flows around two square objects in a special arrangement and tried to reduce the push of the fluid and stop swirling by adding a control object. They also examined the impact of gap spacing and fluid velocity on these effects.

Objectives:

The above-mentioned studies focus on analyzing the flow around various objects in different arrangements to understand the impact of Reynolds number, gap spacing, and aspect

ratio. The Reynolds number greatly influences the flow behavior, changing the stages of flow from steady to unsteady and even transitioning to turbulent behavior at higher values. The gap spacing also plays a vital role in fluid force reduction or extension. Larger gap spacing significantly suppresses vortex shedding, while small gap spacing increases fluid forces. The aspect ratio refers to the size of an object. It also plays a significant role in controlling flow and reducing fluid forces, thereby saving energy. However, there is currently a gap in experimental or numerical data regarding the use of a staggered arrangement with two objects, where one serves as the main object and the other as a control object placed at different locations (top and bottom) of the main object. Therefore, the present study aims to fill this gap by investigating two different configurations of control objects to verify the: i) effect of the Reynolds number on flow control by changing its stages, ii) examination of the configuration of control objects in reducing the fluid forces and to suppress the vortex shedding, iii) determination of Lattice Boltzmann method for saving energy and to control flow to avoid the structure damaging.

Novelty:

This work has great significance in practical engineering applications such as heat exchangers, bridges, chimneys, high-rise buildings, electric ports cooling devices, etc. This study aims to control flow to save energy through two different methods i) Active control method and ii) passive control method, to reduce the fluid forces and suppress the vortex shedding, as the interaction of flow with these objects induces vibrations in the structure. Consequently, vortex shedding occurs, which may devastate the structure.

The current study is structured into different sections, including Introduction, Problem Description and Numerical Method, Grid Independence and Code Validation Study, Effect of Computational Domain, Results and Discussions, and Conclusions.

Problem Description and Numerical Method:

Problem Description:

In this study, two-dimensional (2-D), numerical simulations were performed to analyze the flow over a square object. The configurations are illustrated in Figure 1(a, b), where the first configuration places the control object at the top right corner of the main square object, and the second configuration positions the control object at the bottom right corner of the main object. The dimensions of the main object and control object are represented by d = 20 and d_1 = 20, respectively. The range of Reynolds numbers is selected from Re = 80-200. The upstream distance from the inlet to the main object, denoted as Lup, is set at 7.5d, while the downstream distance from the end of the control object to the exit of the channel, denoted as Ldown, is considered as 28.5d. The dimensions of the channel are represented by L (length) and H (height). The flow is oriented uniformly along the x-axis, so the velocity component is designated as u = U_{inf} and v = 0 at the inlet. In general, two velocity profiles are used in computational flow problems. One is a parabolic profile, where the flow is unconfined and the second one is uniform inflow velocity, where the flow moves inside the channel throughout with the same velocity and is called confined flow. In the parabolic profile, there is a point where the boundary layer occurs, and the maximum velocity is observed. In this study, we used the inflow velocity profile at the inlet, because in confined flow the values of physical parameters are high as compared to unconfined flow, as well as the values of drag and lift coefficients, and that makes the flow turbulent more than that of unconfined flow. Therefore, we selected uniform velocity flow to measure how to control the fluid forces and reduce vortex shedding by using confined flow. No slip boundary conditions (u = 0 = v) are applied to the top and bottom walls of the channel as well as on the surfaces of main and control objects due to their fixed position [23]. The convective boundary conditions are

imposed ($\frac{\partial u}{\partial x} = 0 = v$) at the exit of the channel [23], While the forces acting on main objects can be determined by the momentum exchange method [24].

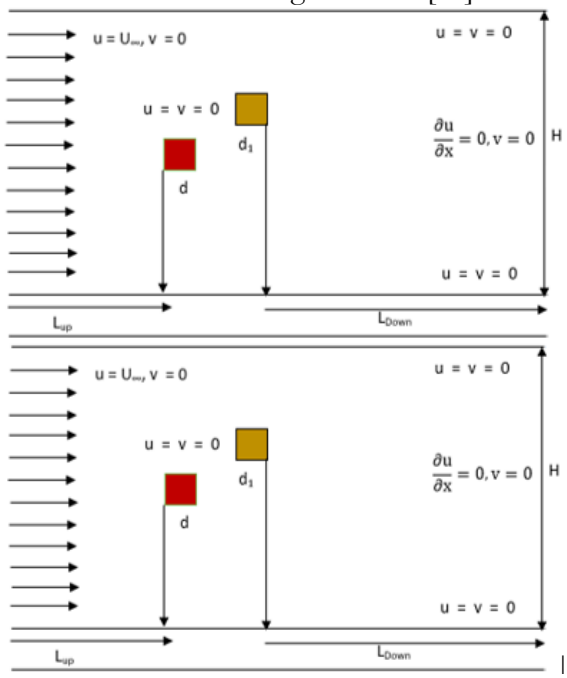

Figure 1: Schematic diagram for flow past over a square object in the presence of control object placed at (a) top and (b) bottom position of the main object.

Numerical Method and Important Parameters:

Lattice Boltzmann Method (LBM) was utilized in this study to solve complex fluid flow problems, including both simple and multiphase flows. This method is based on two different processes, i) Streaming and ii) Collision. The dimensions of the channel are represented by L (length) and H (height). LBM is second-order accurate both in space and time coordinates, is explicit, and converts non-linear terms into linear terms in Navier Stoke equation [25] and [26]. Unlike traditional methods that solve the pressure term using the Poisson equation, LBM utilizes an equation of state $p = \rho c_s^2$, to solve for pressure[26]. Various models are available in LBM, denoted by D_mQn (D is used for dimension and Q is used for several particles. In the present case, the adopted model is D_2Q_9 shown in Figure 2. [27][28][26]. The general equation of the Lattice Boltzmann Method (LBM) in discrete form is

$$g_i(x + e_i\Delta t, t + \Delta t) - g(x,t) = -\frac{\Delta t}{\tau}\left(g(x,t) - g_i^{(0)}(x,t)\right) \quad (1)$$

Here g_i is the density distribution $g_o^{(0)}$ is the corresponding equilibrium density distribution function, $\mathbf{e}_i$ is the velocity of the particle and τ is the stability parameter along time increment Δt. The equilibrium distribution function can be defined and computed as,

$$g_i^{(0)} = \rho\, \xi_i[1+3(\mathbf{e}_i.\mathbf{u})+4.5(\mathbf{e}_i.\mathbf{u})^2-1.5\mathbf{u}^2], \quad i = 0, 1, 2, \ldots, 8 \quad (2)$$

ξ_i are corresponding weighting functions, there values for D_2Q_9 models are $\xi_i = 4/9$ for i = 0, $\xi_i = 1/9$ for i = 1-4 and $\xi_i = 1/36$ for i = 5-8. The physical parameters that we will use in the present problem are, kinematics viscosity of fluid (ν), pressure (p), Reynolds number (Re), drag coefficient (Cd_{rms}), lift coefficient (Cl_{rms}), and Strouhal number (St) can be denoted and calculated as following ways,

$\nu = (2\tau\text{-}1)/6\Delta t$, (3)

$p = \rho c_s^2$

$Re = U_{inf}\, d/\nu$ (5)

$Cd_{rms} = \sqrt{\sum_{t=1}^{n}(Cd(t) - mean\ (Cd(t)^2)/n}$ (6)

$Cl_{rms} = \sqrt{\sum_{t=1}^{n}(Cl(t) - mean\ (Cl(t)^2)/n}$ (7)

$St = Y_s d/U_{inf}$ (8)

Where c_s is the artificial speed of sound and is equal to 0.5774, Y_s is the vortex shedding frequency and n is the total number of time steps [26]. In the case of the convergence test normally two different approaches are used. Firstly, the simulation is terminated once the temporal variation of the lift coefficient becomes periodic. Secondly, one can stop the simulation once the below criteria are satisfied.

$$Error = \frac{\sqrt{\sum_{i,j}\left[\mathbf{u}_{i,j}(t+1) - \mathbf{u}_{i,j}(t)\right]^2}}{\sqrt{\sum_{i,j}\left[\mathbf{u}_{i,j}(t+1)\right]^2}} \leq 5 \times 10^{-8} \quad (9)$$

Grid Independence and Code Validation Study:

Grid Independence Study:

The Grid Independence study is essential for improving the accuracy of results by examining the impact of progressively smaller grid cells, referred to as grid points. The main goal is to transform the continuous domain into a discrete one. To understand the grid point phenomena, the developed code is validated with various grid points including 10d, 16d, 20d, and 24d. These configurations were evaluated to determine the physical parameters Cdmean and Cdrms for both the main object (C1) and the control object (C2) in the flow past the scenario of the object, with a control object positioned at the top right corner and Re = 100, as depicted in Table 1. The values of Cd_{mean} for C1 and C2 at 20d and 24d were approximately the same as compared to 10d and 16d, with values of 1.5934 and 1.5932, respectively and some minor differences in Cd_{mean} values were noticed for 10d and 16d. Similar behavior was observed for Cd_{rms} values for C1 and C2 objects. The values of Cd_{rms} were very close at 20d and 24d, which are 0.3157 and 0.3144 in contrast to 10d and 16d. The differences are presented in Table 1. However, in comparison between 20d and 24d, we selected 20d because it takes less computational time and is not as cost-effective as 24d to Cd_{mean} and Cd_{rms}. Therefore, to obtain better and more accurate results in terms of convergence and computational time, we used Eq.9 to check the accuracy of grid points. Therefore, we utilized 20d grid points for conducting all simulations of the present problem. [29] also suggested using 20d grid points for convergence.

Table 1: Grid Independence Study for flow Past a main object in the presence of a control object at the top right corner for Re = 100

Grid Points	=10d	=16d	=20d	=24d
$Cd_{mean}1$	1.4929	1.5797	1.5934	1.5932
$Cd_{mean}2$	1.5358	1.7584	1.8049	1.8049
Cd_{rms} 1	0.0763	0.1103	0.3144	0.3132
Cd_{rms} 2	0.0933	0.1072	0.3157	0.3144

Code Validation Section:

The Code Validation Study is a crucial step in ensuring the accuracy and reliability of code for solving the problem. In this study, we simulated the flow past a single square object at three different values of Reynolds number i.e. Re = 100, 150, and 200 by using Lattice Boltzmann Method (LBM) (see Figure 2(a, b)). The values of physical parameters Cd_{mean} and St are calculated and shown in Figure 2(a, b). At Re = 100, 150, and 200, the obtained values of Cd_{mean} are 1.42, 1.40, and 1.45 respectively. Similarly, the calculated values of St are 0.143, 0.155, and 0.151 as shown in Figure 2(a). The results experimentally and numerically obtained by different scientists at values of Re = 100, 150, and 200 having different numerical schemes and grid points by using the flow past over a single square cylinder were compared with the results obtained from the present problem. We obtained the values of physical parameters such as Cd_{mean} and St and compared the results of Cd_{mean} with available experimental and numerical data in the literature, the values of Cd_{mean} were very close to the mean drag value obtained by [30][31], and [32] at Re = 100 instead of [33], that are 1.447, 1.46 &1.4. Similarly, the Cd_{mean} value of the present result identified similar values with [34][30], and [31] at Re = 150 which are 1.45, 1.443 &1.41. At Re = 200, the mean drag coefficient values of the present results show close agreement with the results obtained by the study [34] and [31], which are 1.42 & 1.49. Additionally, the values of Strouhal number (0.145, 0.156 and 0.152) obtained from our simulations were compared with available data in the literature at Re = 100, 150, and 200, showing good agreement with results from [30], [16] and [23] and those results are (0.144, 0.144 & 0.141 at Re = 100, 0.155, 0.156 & 0 at Re = 150 and Re = 200 the available values are 0, 0, 0.151, respectively (see Figure 2(b)). These comparisons validate the accuracy of our code and demonstrate its capability to produce reliable results consistent with already published literature.

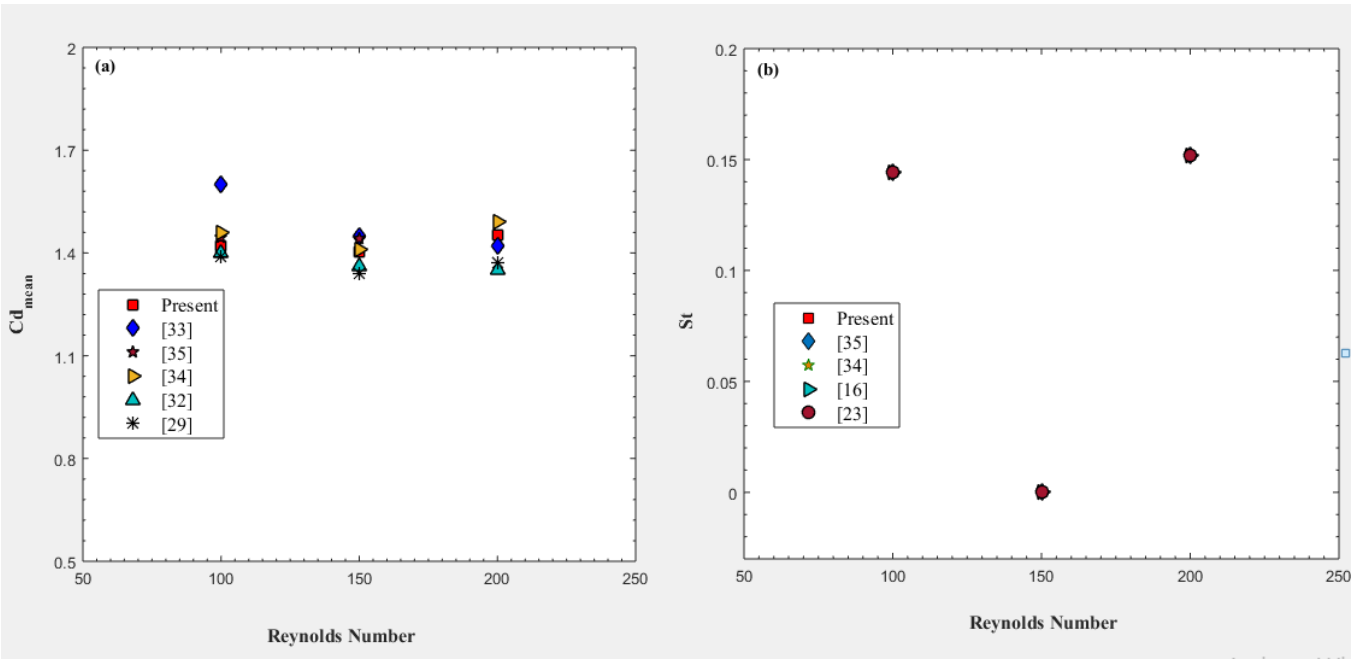

Figure 2: (a, b). Code validation study at Re = 100, 150, and 200 for flow past a single square object.

Effect of Computational Domain:

Table 2: Effect of Computational Domain for flow past over a main object in the presence of control object at top right corner for Re = 160

Cases	L_{up}; L_{Down} ; H	$Cd_{mean}1$	$Cd_{mean}2$	$Cl_{rms}1$	$Cl_{rms}2$	St1	St2
I	L_{up} = 5d; L_{down} = 29.5d; H = 11d	1.672	2.052	0.178	0.904	0.001	0.129

II	L_{up} = 7d; L_{down} = 29.5d; H = 11d	1.670	2.053	0.177	0.900	0.002	0.130
IV	L_{up} = 11d; L_{down} =29.5d; H = 11d	1.573	1.930	0.192	0.816	0.0013	0.125
V	L_{up} = 9d; L_{down} = 24.5d; H = 11d	1.568	1.863	0.174	0.663	0.0013	0.122
VI	L_{up} = 9d; L_{down} = 27.5d; H = 11d	1.551	1.908	0.186	0.719	0.0013	0.121
VII	L_{up} = 9d; L_{down} = 29.5d; H = 11d	1.549	1.903	0.176	0.709	0.0013	0.132
VIII	L_{up} = 9d; L_{down} = 31.5d; H = 11d	1.551	1.907	0.184	0.717	0.0013	0.133
IX	L_{up} = 9d; L_{down} = 29.5d; H = 6d	1.988	2.658	0.290	1.174	0.0013	0.150
X	L_{up} = 9d; L_{down} = 29.5d; H = 8d	1.738	2.235	0.208	0.993	0.0013	0.140
XI	L_{up} = 9d; L_{down} = 29.5d; H = 9d	1.669	2.104	0.185	0.918	0.0013	0.132
XIII	L_{up} = 9d; L_{down} = 29.5d; H = 13d	1.527	1.848	0.184	0.769	0.0013	0.126

The process of selecting a suitable computational domain involves exploring different values of upstream (L_{up}), downstream (L_{Down}), and height (H) of the channel at Re = 160 for flow past a square object in the presence of a control object placed at right bottom corner of the main object. The values of physical parameters such as Cd_{mean}, Cd_{rms}, and St for both objects are calculated as shown in Table 2. At fixed values of L_{Down} and H, and by changing the values of upstream distance, we noticed that the smallest value of Cd_{mean} is obtained at L_{up} = 9d and 13d along with L_{Down} = 29.5 for both C1 and C2. The values of Cl_{rms} are approximately equal to each other at all selected values of upstream distance. Similarly, it is observed in the case of Strouhal number by taking L_{up} = 5d, 7d, 9d, and 11d. Now by fixing the values of upstream (L_{up}) distance and height (H) of the channel and by varying the values of downstream distances (L_{down}) i.e. 24.5d, 27.5d, 29.5d, and 31.5d, respectively. The values of mean drag coefficients for both objects are smallest at L_{Down} = 29.5d and H = 13d with L_{up} =11d as compared to other chosen values except H = 6d, 8d, and 9d, respectively. Additionally, the Cdrms values approached each other at all L_{Down} distances, indicating stability in the flow patterns. The smallest St value of 0.121 for C2 was observed at LDown = 29.5d. Lastly, we compared the values of the height of the channel at H = 6d, 8d, 9d, 11d, and 13d at fixing the values upstream and downstream distances at L_{up} = 9d and L_{Down} is 29.5d. The smallest value of Cd_{mean} is obtained at H = 11d and 13d. The same behavior is examined for the case of Cl_{rms} and St values. Comparing 11d and 13d, 13d takes much time for computation. Based on these results and considerations, the optimal values selected for Lup, LDown, and H are Lup = 9d, LDown = 29.5d, and H = 11d. These values are determined based on the smallest Cdmean values and computational efficiency, as detailed in Table 2 and the described analysis.

Results and Discussions:

We conducted a two-dimensional (2-D) numerical study for flow past a main object in the presence of a control object of the same size ($d = d_1 = 20$) placed at the top and bottom right corners of the main object. Our primary objective was to analyze the impact of varying Reynolds numbers on the flow characteristics surrounding these configurations, with a specific focus on understanding the flow structure mechanisms. Moreover, our study aimed to elucidate the effectiveness of each configuration in controlling flow dynamics and mitigating vortex shedding, particularly concerning different Reynolds numbers. We obtained results in terms of vorticity contours, drag and lift coefficients, and physical parameters. In the vorticity contour, solid lines represent the positive vortices, while dashed lines denote the negative vortices. To streamline the presentation and focus on significant findings, we selected a few cases that exhibited distinct behavior omitting those with similar outcomes to avoid redundancy.

Wake Structure Mechanism:

In the vorticity contour visualization for the first configuration, (where the control object was placed at the bottom right corner of the main object) under the effect of Re = 80-200, we observed three different flow behaviors. At Re = 80-100, the shear layer emerging

from the top and bottom corners of the main objects moves downstream independently, without attaching to the shear layer of the bottom control object. As the flow progressed, the shear layer of both the main and control objects rolled up and started a rotational motion of the flow at the downstream location, leading to the formation of vortex shedding at the middle position of the computational domain. Negative vortices appear from the main objects, and positive vortices are generated from the control object. These positive and negative vortices move in an alternate way to form a von Karman vortex street, as shown in Figure 3(a). Notably, there was no merging of vortices observed throughout the domain, and all shed vortices exhibited a rounded shape. When the Reynolds number is increased from Re = 100 to 120, another behavior of vortex shedding is observed. In this flow behavior, both positive and negative vortices generated from the main and controlling objects move parallel to each other in the form of two rows instead of an alternate way. Therefore, the von Karman vortex street transforms into a two-row vortex street at Re = 120 only (see Figure 3(b)). As the Reynolds number continued to increase beyond Re > 120, a critical shift in vortex-shedding behavior became apparent. The vortices generated from the main objects, having no regular pattern, are mixed up with irregular vortices shed from the control object. Their shapes and sizes also vary, with some being oval-shaped and few having a round shape (see Figure. 3(c, e)). Therefore, this flow behavior is termed the critical behavior of the flow.

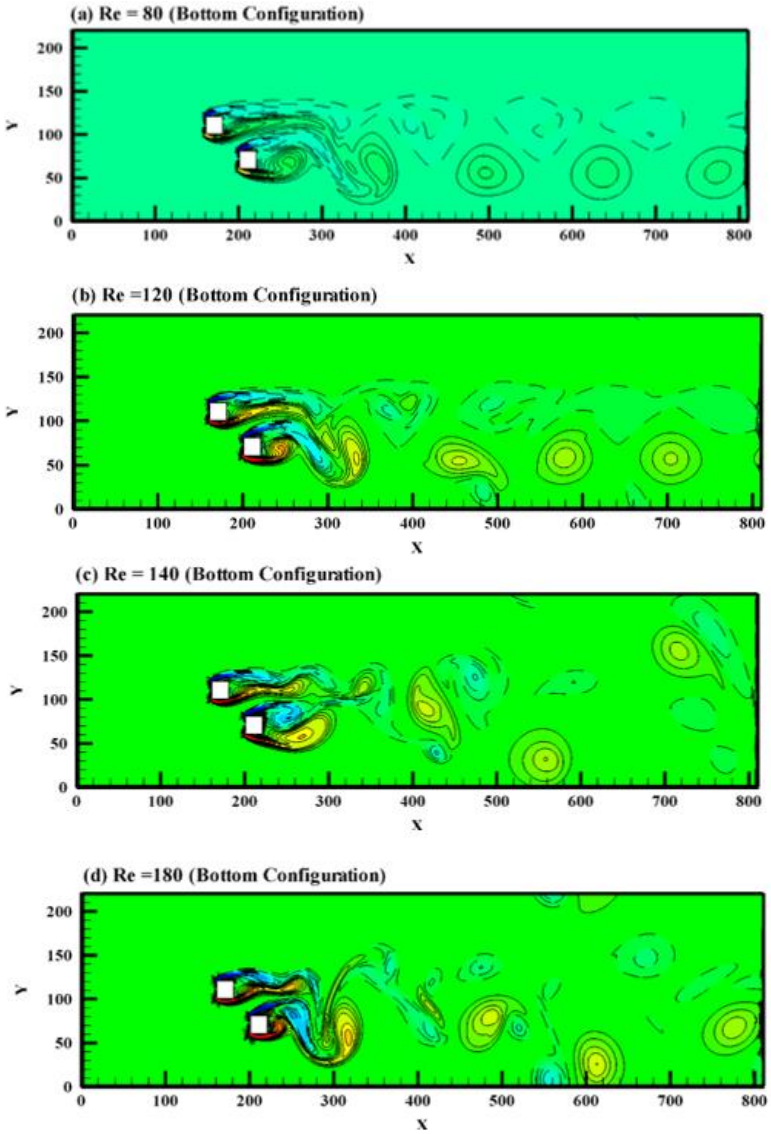

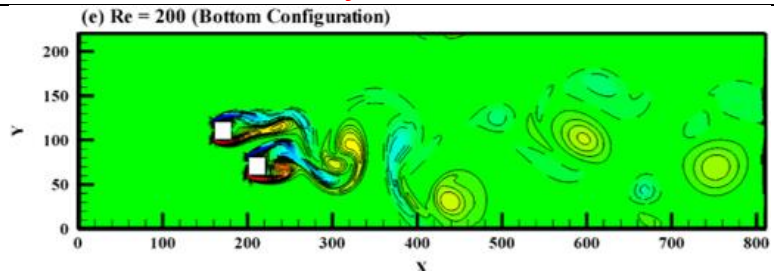

Figure 3 (a, e): Vorticity contour for flow past a square object in the presence of control object placed at the bottom right corner

The time trace analysis of drag and lift coefficients is shown in Figure 4(a-p). For the first flow behavior known as Von Karman vortex street flow mode existing at Re = 80-100, the drag and lift coefficients represented the periodic behavior for the main objects (C1) due to alternate vortex shedding. However, for C2, the drag coefficient is modulated due to changes in the size and shape of shed vortices, and the lift coefficient is periodic for both selected Reynolds numbers, i.e., Re = 80-100. The drag coefficient is the force acting in the horizontal direction and depends on the shape and size of the vortices. If vortices are changed in shape and size then drag automatically becomes modulated instead of representing the periodicity. The lift coefficients will be periodic only for the case when an alternate vortex is generated and moves in an alternate way. The modulation in the drag coefficient for C2 is decreased with an increment in Reynolds number values from 80 to 120. The Reynolds number, is greatly influenced by changing the flow stages, from steady to transition at low to moderate range of Reynolds number and from transition to turbulent stage of flow at medium range of Reynolds number to high value of Re. The magnitudes of drag and lift coefficients also decreased with an increment in the range of Reynolds numbers. The Cd and Cl for the second observed flow behavior, are known as two rows vortex street flow mode, where two parallel rows of vortex shedding are examined, exhibiting periodic drag and lift coefficients for C1 and modulated drag coefficient for C2 with periodic lift coefficient. In the third observed flow behavior of vortex shedding, known as chaotic flow behavior, the drag and lift coefficients for both C1 and C2 are modulated due to irregularities in shed vortices, as shown in Figure 4. The magnitudes of Cd and Cl increase with an increase in Reynolds number.

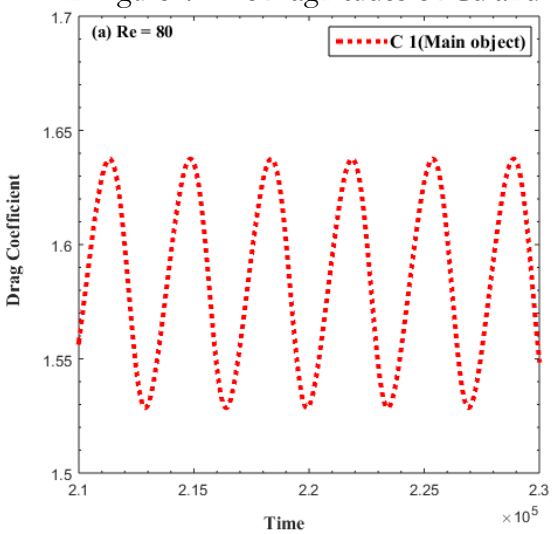

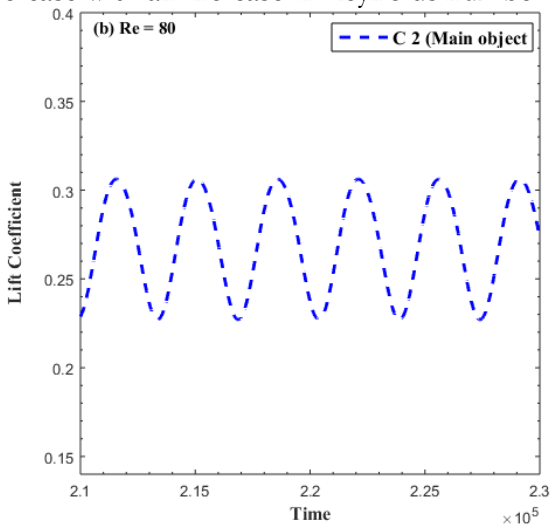

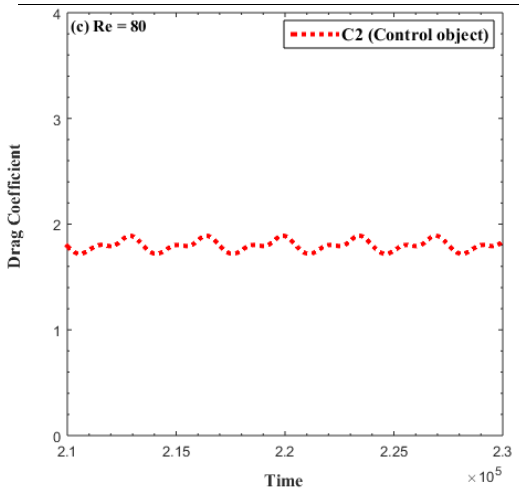
(c) Re = 80
C2 (Control object)
Drag Coefficient
Time
×10^5

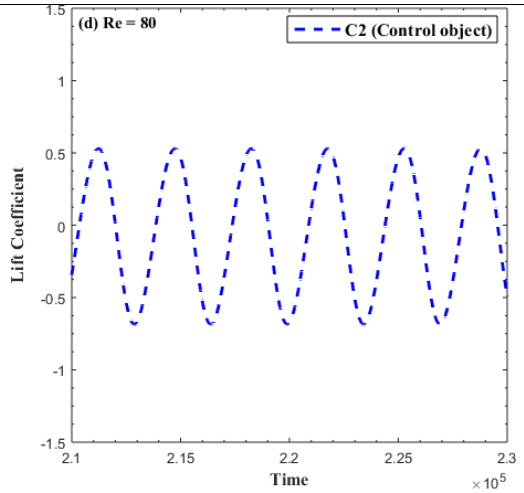
(d) Re = 80
C2 (Control object)
Lift Coefficient
Time
×10^5

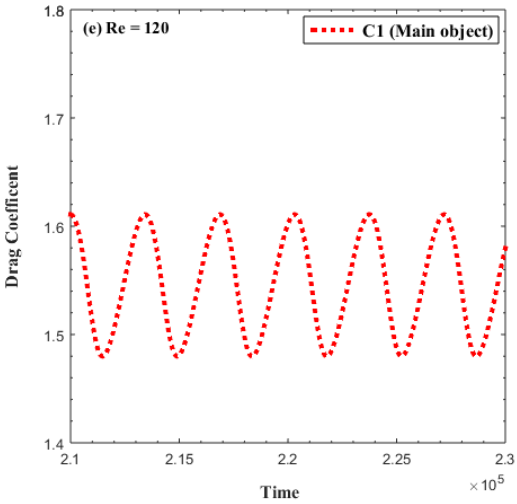
(e) Re = 120
C1 (Main object)
Drag Coefficent
Time
×10^5

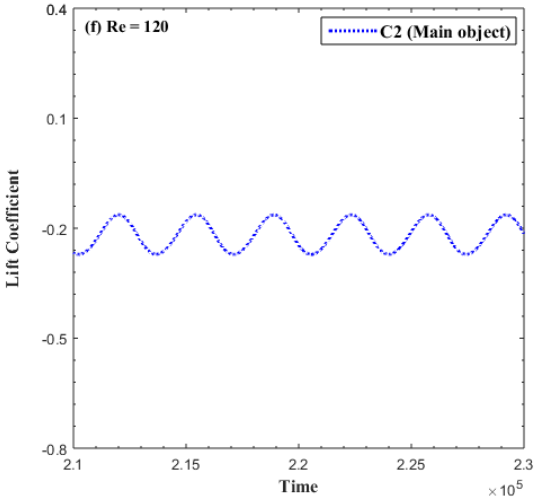
(f) Re = 120
C2 (Main object)
Lift Coefficient
Time
×10^5

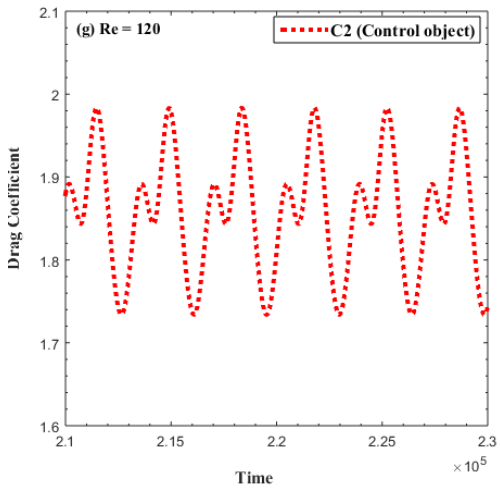
(g) Re = 120
C2 (Control object)
Drag Coefficient
Time
×10^5

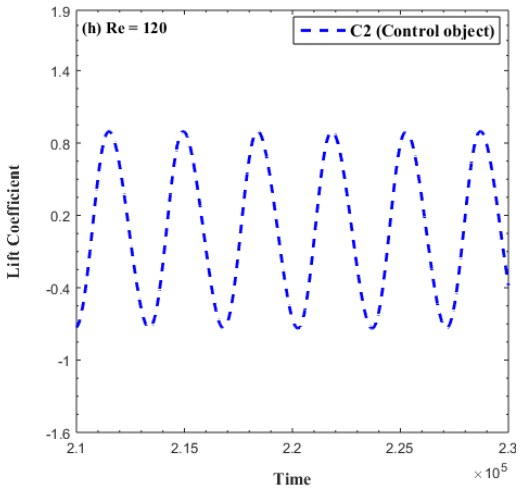
(h) Re = 120
C2 (Control object)
Lift Coefficient
Time
×10^5

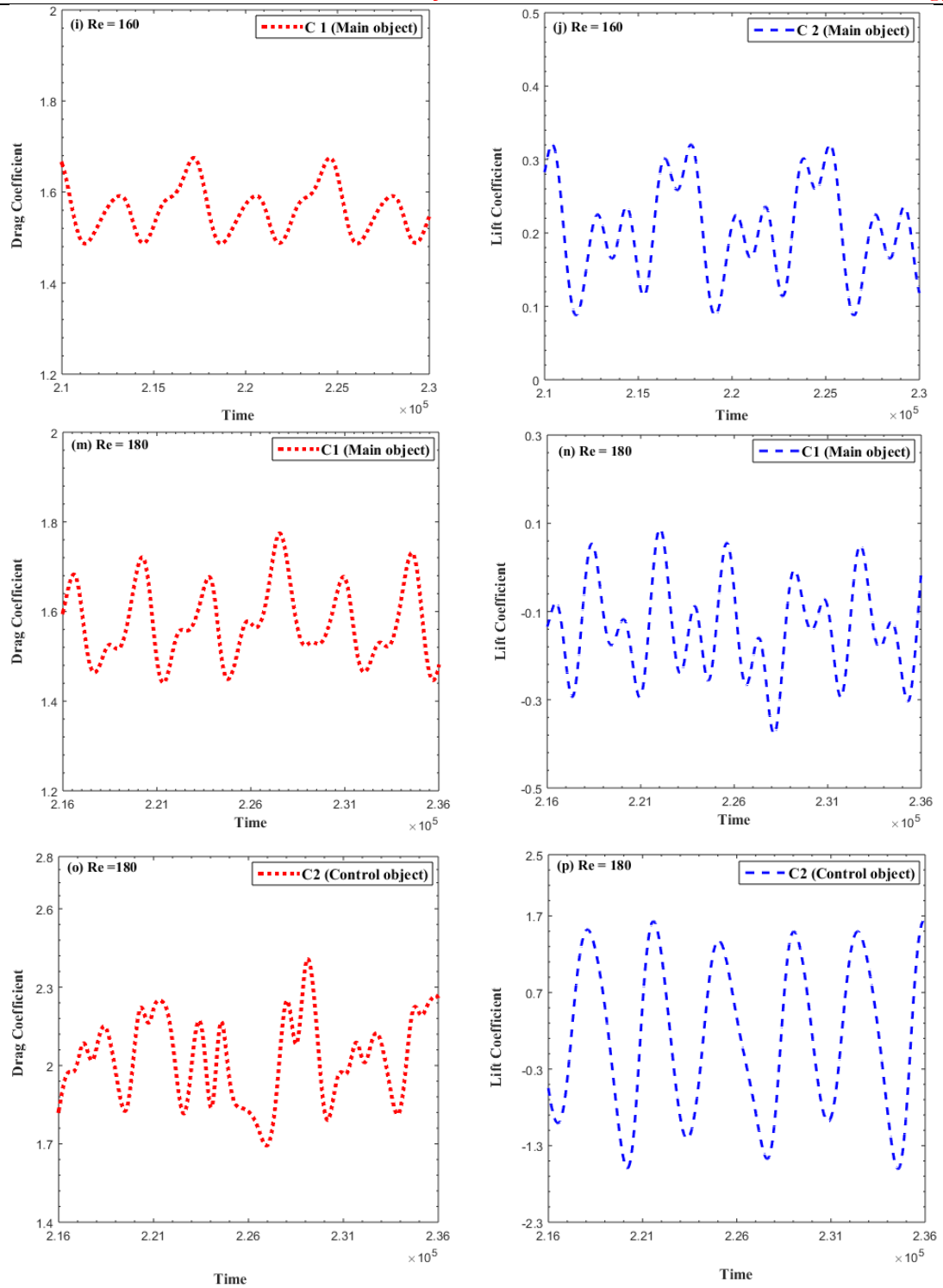

Figure 4 (a, p): Drag and Lift Coefficient for flow past a square object in the presence of control object placed at the bottom right corner

The vorticity contour visualization for the second configuration, where the control obstacle is placed at the top right corner of the main obstacle, reveals two different flow behaviors. The first flow behavior is observed at Re = 80-100, as shown in Figure 5(a), where the shear layer emerges from the top controlling cylinder combined with the main obstacle shear layer. With the combination of these two layers, an irregular flow behavior is observed in the near-wake region. No proper vortex shedding is identified initially, but after some time,

both negative and positive vortices appear at the downstream location. Negative vortices are shed from the top controlling obstacle, and positive vortices are shed from the main obstacle, moving alternately. However, their sizes and shapes are quite different due to drag force frequency, which decreases or increases due to the pressure effect. Some small bubbles also appear at Re = 100. At Re = 120-200, the flow behavior is regularly disturbed. At the high range of Reynolds numbers, the fluid molecules start to move fast and interact with each other and create collision among themselves due to high velocity, which disturbs the flow and causes the merging of vortices. Merging and distortion are identified in vortex shedding. In the near-wake region, a slight merging of vortices is identified, but as the distance increases from downstream of the main and control obstacle, irregularities increase. Shed vortices spread all over the computational domain with high and low frequencies of shed vortices. The flow behavior is known as critical, as the range of Reynolds numbers increases from Re = 140 to 200, the critical behavior of the flow also approaches its extreme position. No one can identify the vortices that are generated from different obstacles. Therefore, this flow behavior is known as a critical flow behavior.

The time trace analysis of drag and lift coefficients for the second configuration is shown in Figure 5(a-d). The drag and lift coefficients for cases at Re = 80-100, represented the periodic behavior for C1 and C2, except the drag coefficient of C2, which is somewhere modulated due to various sizes of vortices generated from both objects. However, this modulation was less pronounced for Re = 100. The magnitudes of Cd and Cl for the control object are larger than those for the main object. The magnitude of drag and lift coefficients for the critical flow behavior of the object placed at the top right corner is shown in Figure 6(a-p). The Cd and Cl for all cases included in critical flow behavior are modulated for both the main and control objects. As the value of the Reynolds number is increased from 120 to 200, the rate of modulation in drag and lift coefficients is also increased and approaches extreme irregularity. In comparison between C1 and C2, drag and lift coefficients are more modulated for C2 than for C1. Furthermore, the magnitudes of drag and lift coefficients are also increased with Reynolds number.

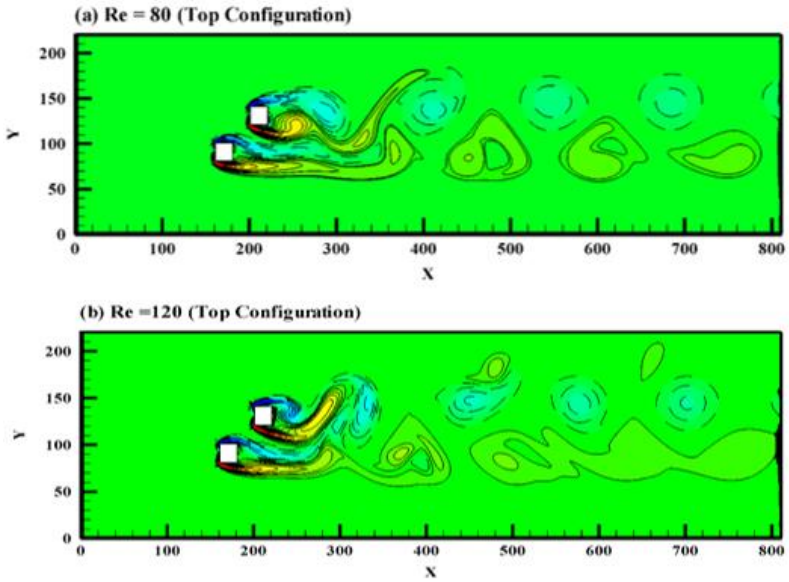

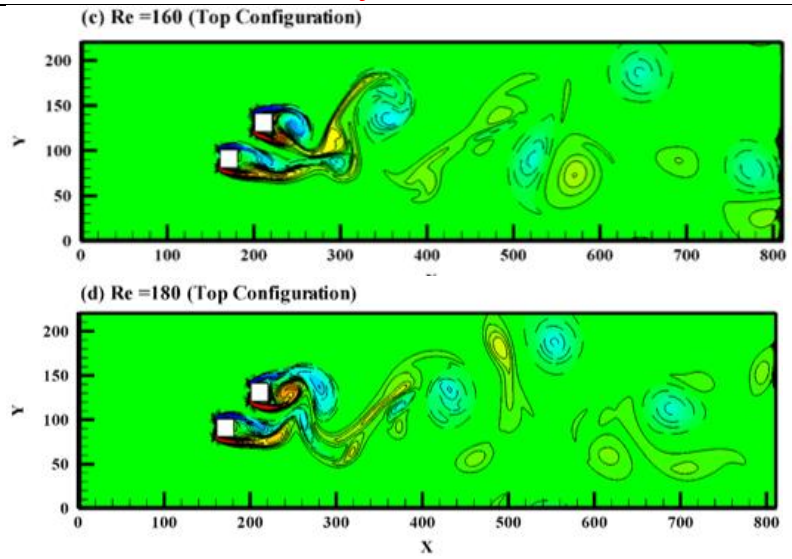

Figure 5 (a, d): Vorticity contour for flow past a square object in the presence of control object placed at the top right corner

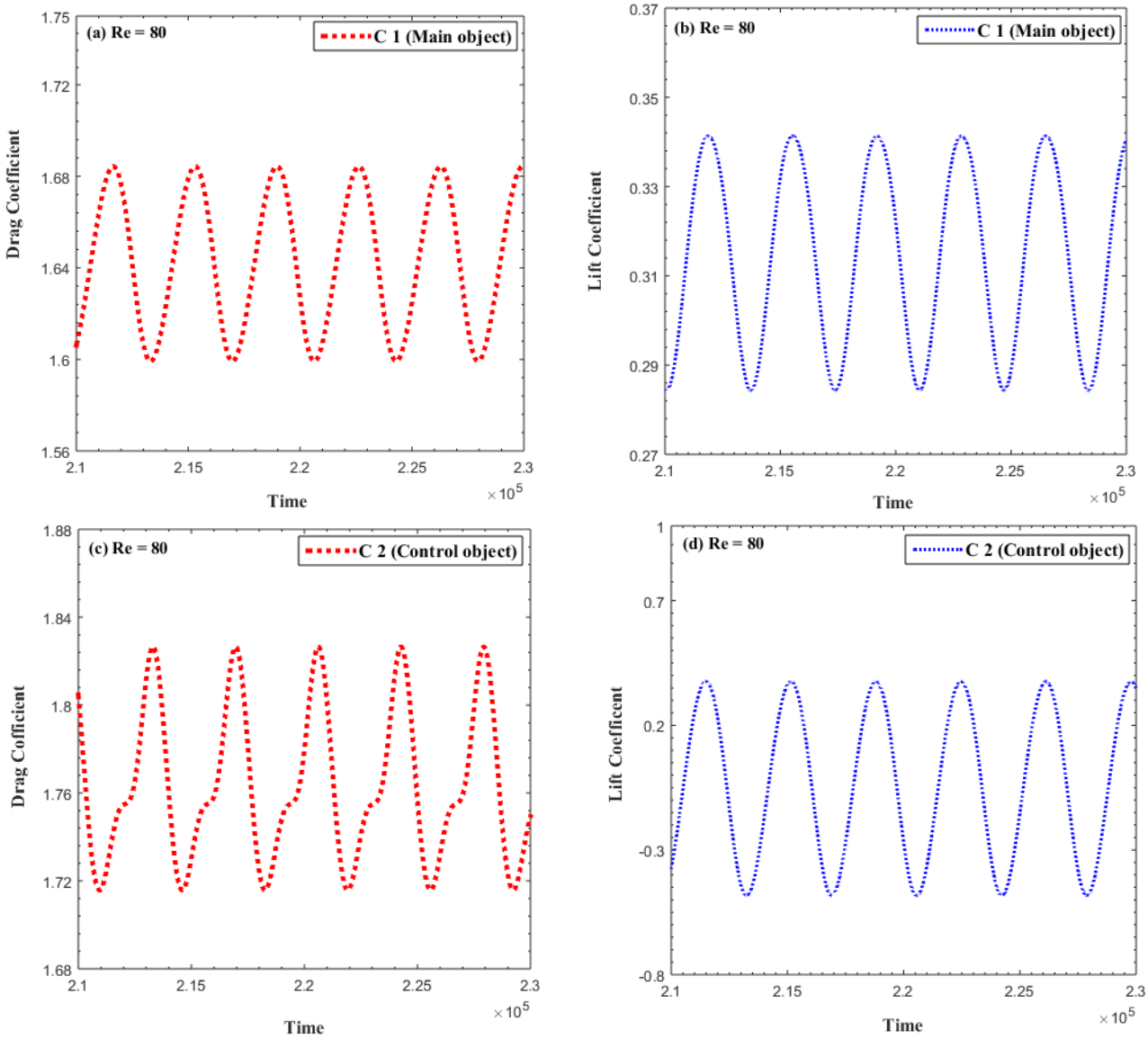

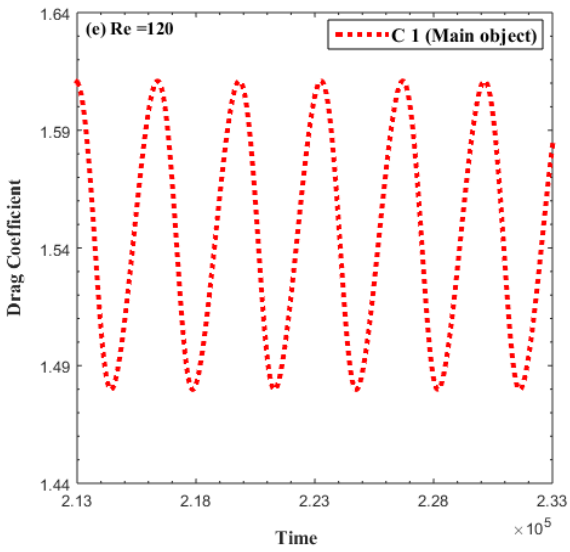
(e) Re =120
C 1 (Main object)
Drag Coefficient
Time
×10^5

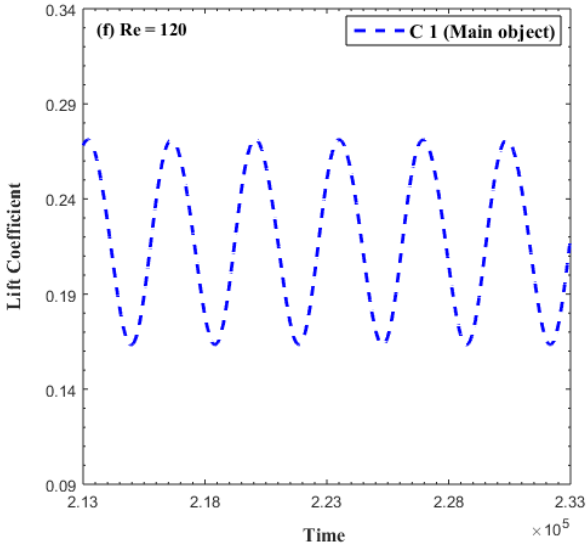
(f) Re = 120
C 1 (Main object)
Lift Coefficient
Time
×10^5

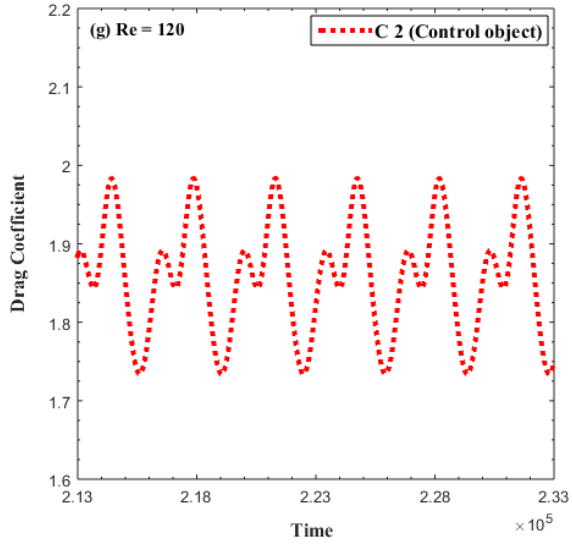
(g) Re = 120
C 2 (Control object)
Drag Coefficient
Time
×10^5

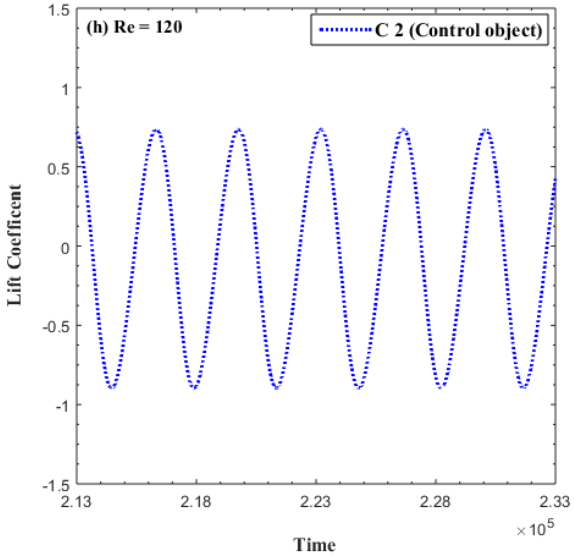
(h) Re = 120
C 2 (Control object)
Lift Coefficient
Time
×10^5

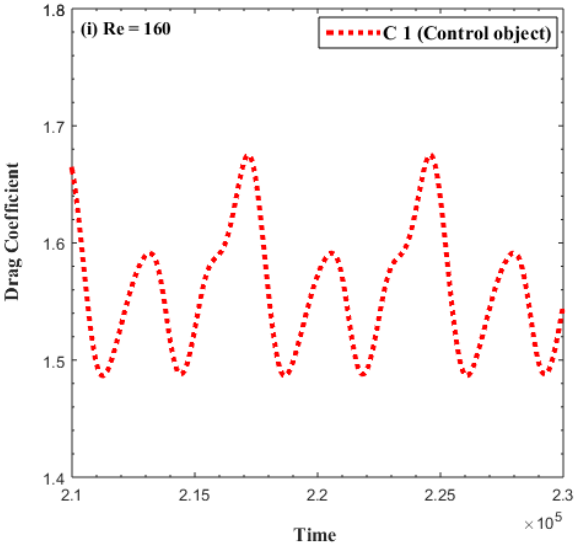
(i) Re = 160
C 1 (Control object)
Drag Coefficient
Time
×10^5

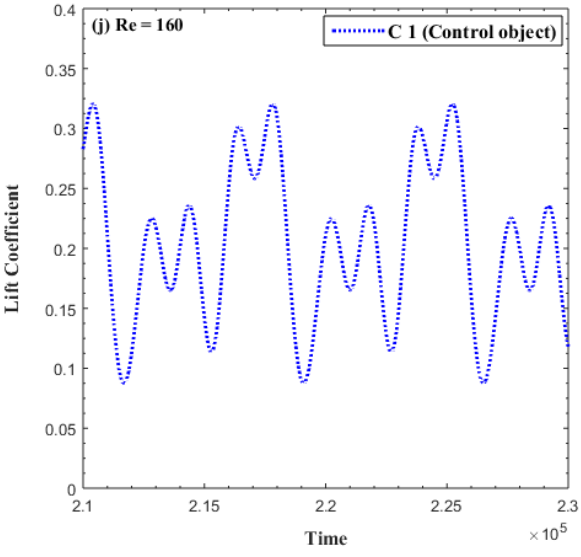
(j) Re = 160
C 1 (Control object)
Lift Coefficient
Time
×10^5

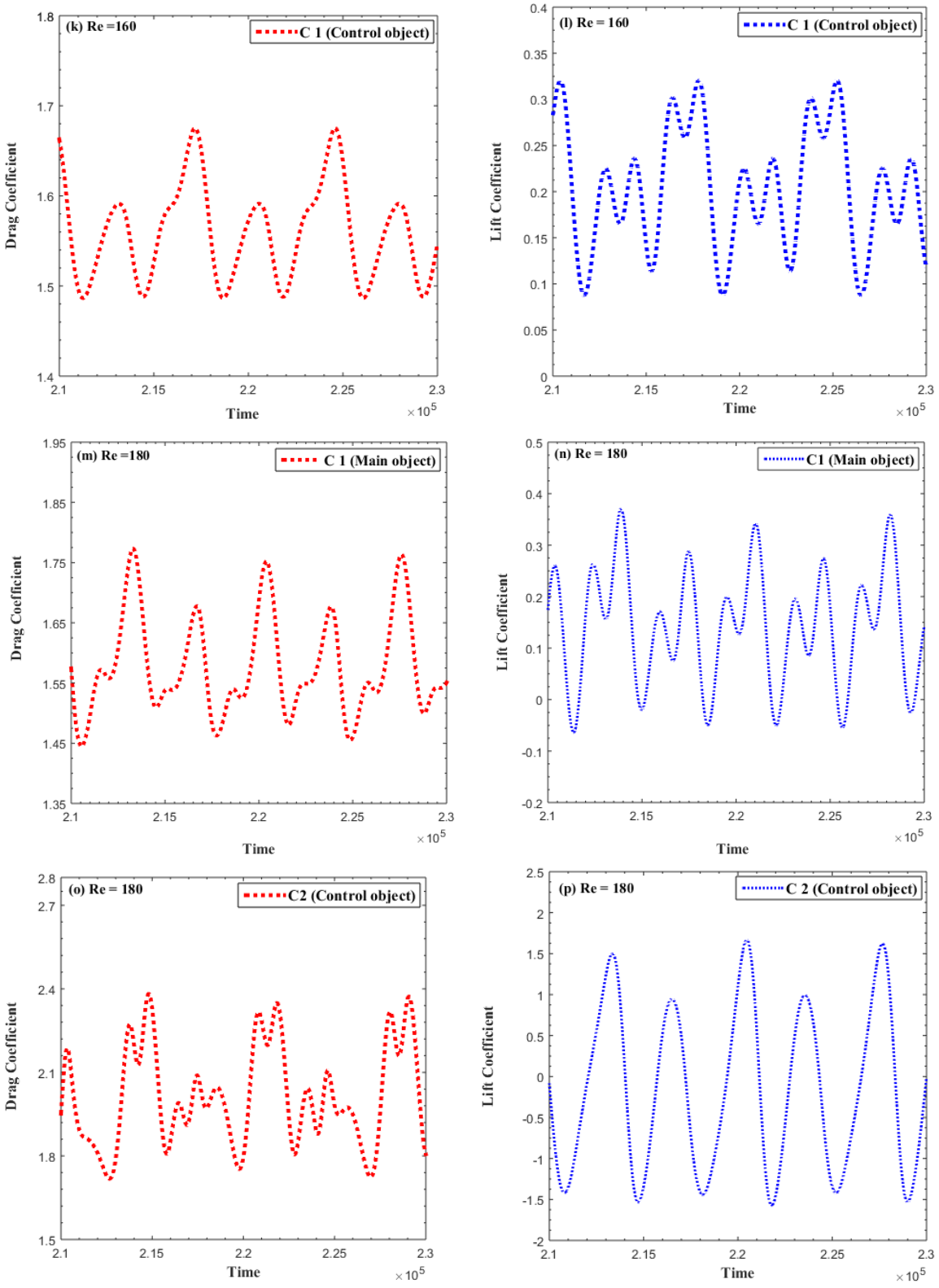

Figure 6(a, p): Drag and Lift Coefficient for flow past a square object in the presence of control object placed at the top right corner

Physical Parameters:

A study of 2-D incompressible flow past two square objects in two different configurations at various Reynolds numbers (Re = 80 – 200) was conducted to examine the

behavior of physical parameters such as Cd_{mean}, Cd_{rms}, Cl_{rms}, and St, at a fixed distance as shown in Figure 7(a, d). The value of Cd_{mean} for the first configurations, where the second object is placed at the top-right corner of the first object, is decreased from Re = 80-160 and then starts to be increased from Re = 180-200 for object C1 (see Figure. 7(a)). However, for object C2 positioned in the top-right corner, the mean drag coefficient values started to increase continuously from Re = 80-200, without any moderate fluctuation. The maximum mean drag coefficient value from both objects for the first configuration is acquired at Re = 200, and it is 2.0708. While considering the second configuration, the value of Cd_{mean} observed for the first C1 decreased from Re = 80-120 and started to be increased at Re = 140-200.

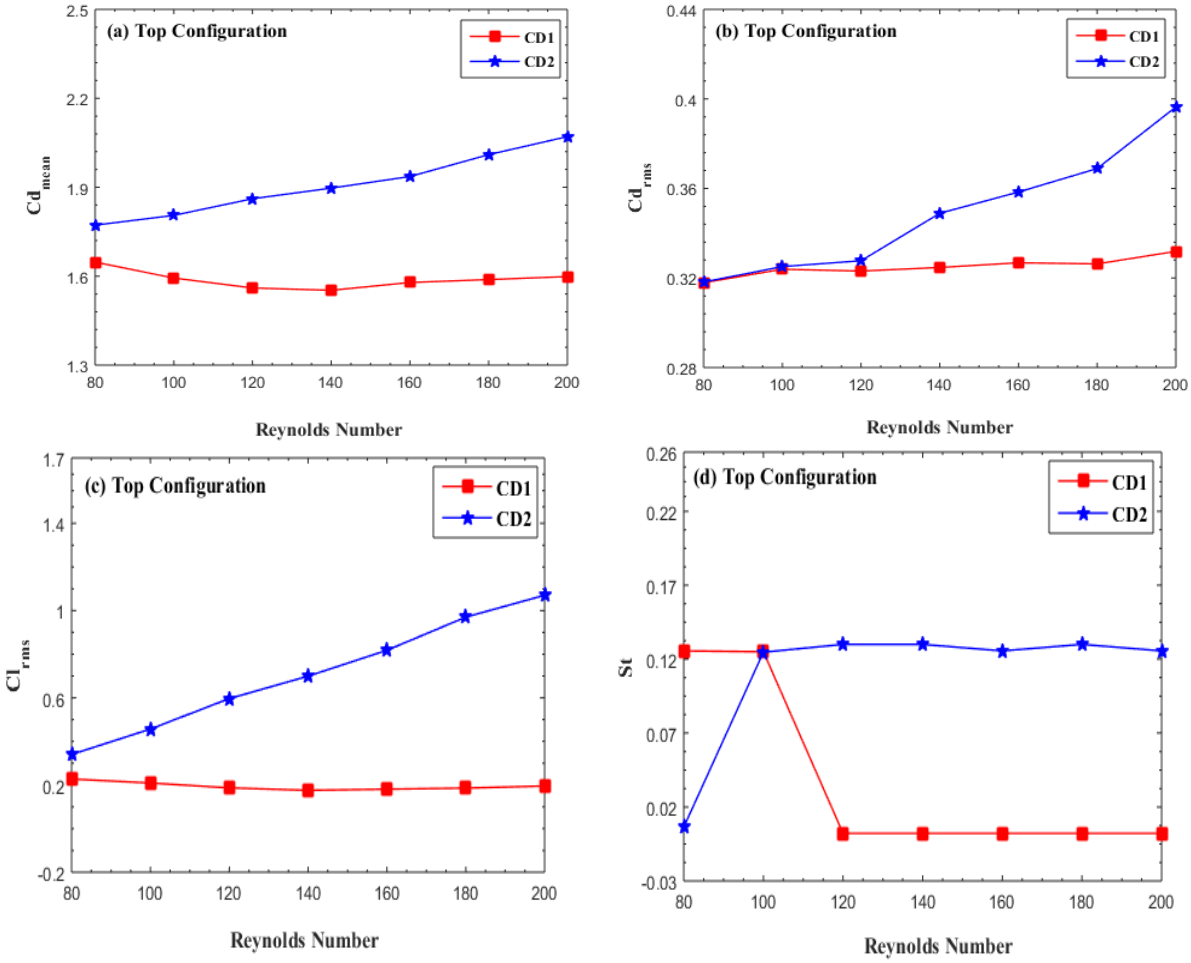

Figure 7(a, d): Physical parameters (a) Cd_{mean}, (b) Cd_{rms}, (c) Cl_{rms}, and (d) St for First Configuration, where C2 is placed in the top right corner.

In the second object C2, placed at the bottom right corner of the first object, the mean drag coefficients are increased by increasing the Reynolds number from Re = 80-120. After that, from Re = 140-200, the mean drag coefficients represented a mixed trend, sometimes increasing or decreasing with increasing Reynolds number. This behavior of Cd_{mean} is different from the first configuration of C2 (see Figure 8(a)). The greatest value of Cd_{mean} from both objects is found at Re = 180, with a value of 2.0015.

In the comparison of both configurations concerning the mean drag coefficient, a very minute difference was observed in the maximum value of Cd_{mean}. For the first configuration, it is 2.0708, but for the second configuration, where the second object was at the right-bottom side, it is 2.0015. The value of Cd_{rms} for both the first and second objects lie in the first configuration where the second object is placed at the top-right corner of the first object, as shown in Figure 7(b). The root means square values of drag coefficients for both the first and

second objects show a mixed trend, sometimes increasing or decreasing with an increment in Reynolds number. The greatest value of Cd_{rms} for C1 and C2 is observed at Re = 200, i.e., 0.3964 for C2 as compared to C1. In the second configuration, where C2 is at the bottom-right corner of C1, the root means square values of drag coefficients are decreased from Re = 80 to 140 (see Figure 8(b)). Afterward, from Re = 160 to 200, Cd_{rms} values represented a mixed trend for both C1 and C2. This phenomenon of Cd_{rms} for the second configuration is quite different from the first configuration, where Cd_{rms} represented a mixed trend. The maximum value of Cd_{rms} for C1 and C2 is found at Re = 200, and it is 0.4011, obtained for C2 in comparison to C1. In the comparison of both configurations, Cd_{rms} for the case where the second object is placed at the right-bottom corner shows distinct behavior.

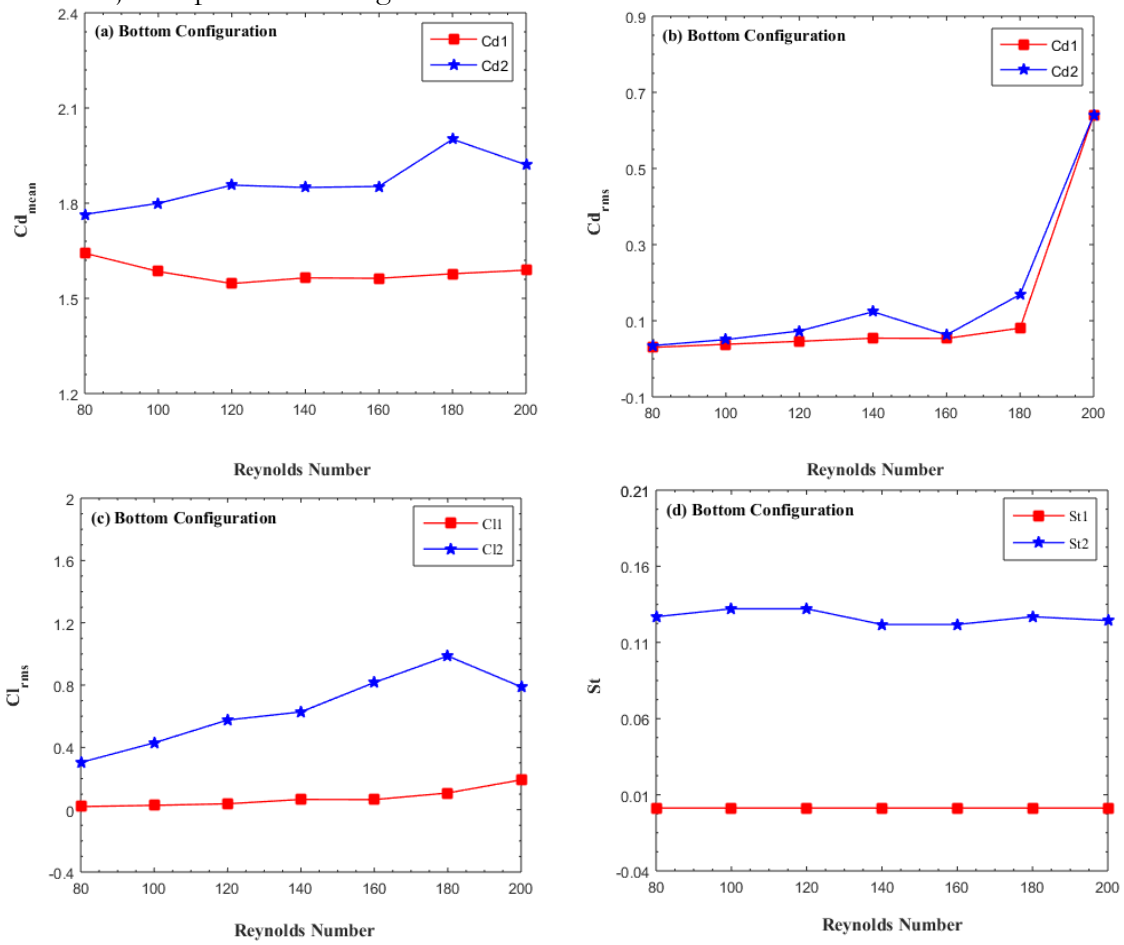

Figure 8(a, d): Physical parameters (a) Cd_{mean}, (b) Cd_{rms}, (c) Cl_{rms}, and (d) S_t for the second configuration, where C_2 is placed in the bottom right corner.

The root mean square values of lift coefficients for both configurations are shown in Figure 7(c) and Figure 8(c). The Cd_{rms} for the first configuration of C1 decreased from Re = 80-140 and then started to increase from Re = 160 to 200. For C2, the root mean square values of lift coefficients are increasing with an increment in Reynolds number from Re = 80-200 without any fluctuation. The maximum value of Cd_{rms} for both C1 and C2 for the first configuration, where C2 is placed at the top-right corner of C1, is 1.0704 found at Re = 200 for C2, respectively. In the second configuration, where C2 is placed at the bottom-right corner of C1, the Cd_{rms} values are decreased from Re = 80-140 and then increased from Re = 160 – 200. For C2, the Cl_{rms} values increased from Re = 80-180, however, after a while, it started to be increased at Re = 200. The behavior of Cl_{rms} for C1 is consistent for both configurations but opposite for C2. The maximum value of Cl_{rms} for the second configuration

is obtained for C2 at Re = 180, with a value of 0.9871, which is comparatively less than the first configuration.

The energy spectrum analysis (St) for both configurations is represented in Figures 7(d) and 8(d). For the first configuration, where C2 is placed at the top-right corner of C1, the values of the Strouhal number are represented in Figure. 7(d). The Strouhal number values for C1 are decreased from Re = 80-100, after that, it has a constant magnitude of 0.0022 for C1. But for C2, it has shown an increasing behavior from Re = 80-140 and then represented a mixed trend for higher Reynolds numbers. The maximum value of St is obtained at Re = 120 and 180, which is 0.1300. For the second configuration, the St values for C1 represent a constant behavior for all selected values of Re = 80 – 200. For C2, the Strouhal number at smaller values of Re = 80-120 is represented by an increasing and then decreasing trend at larger values of Reynolds numbers from Re = 140-200 as shown in Figure 8(d). The maximum value from both objects was obtained for C2, with a value of 0.1321 at Re = 100 and Re = 120.

Conclusions:

A numerical study was conducted to investigate the flow structure mechanism and to reduce fluid forces under the influence of control objects placed at the top and bottom right corners of the main object, covering a range of Reynolds numbers (Re = 80-200). The numerical technique employed was the Lattice Boltzmann Method (LBM). The problem was divided into two different parts. Firstly, suitable grid points were examined, along with the study of the computational domain, considering different values of upstream and downstream locations and the height of the channel. An appropriate computational domain was selected for the present problem. To validate the code, the obtained results for Re = 100, 150, and 200 were compared with available results in the literature, either experimental or numerical, to ensure the validity of the present code. Subsequently, the effect of the Reynolds number under both configurations was studied in terms of vorticity contour, drag and lift coefficients, and physical parameters at fixed gap spacing between both objects i.e. g = 1d. The following observations were made:

- For the configuration where the control object is placed at the bottom right corner, three different flow behaviors were observed: regular behavior (shear layer and two rows vortex street) at small and medium values of Reynolds number and irregular/chaotic behavior (critical flow) for larger values of Reynolds number.
- For the second configuration, where the control object is placed at the top right corner, only two types of flow behavior were observed: regular flow behavior at Re = 80 and 100 and critical flow behavior at Re = 120-200.
- In the calculation of the mean drag coefficient, it was observed that for both configurations, the main object (C1) has a Cd_{mean} value that decreased at Re = 80 to 140, then started to increase with an increment in Reynolds number values from Re = 160-200. The opposite phenomenon was observed for the controlling object, where the Cd_{mean} continually increased with an increment in Reynolds number values.
- The maximum value of Cd_{mean} was obtained for the case where the control object is placed at the top right corner at Re = 200, and it is 2.0708 for C2 as compared to C1 (main object).
- The maximum values of Cd_{rms} were examined for the configuration in which the control object is at the top right corner at Re = 200, and it is 0.6408 obtained for the control object.
- vii) The maximum values of Cl_{rms} were found for the configuration in which the control object is at the top right corner, and at Re = 180, it was 0.9871 for C2.

- The Strouhal number showed constant behavior for C1 at Re = 120-200 for the first configuration in which the control object is at the top right corner. However, St values for C2 exhibited a mixed trend.
- The maximum values of the Strouhal number were examined for C2, and its value was 0.1321 at Re = 100 & 120.

From all the above-mentioned points, it is noticed that physical parameters contain maximum values for configuration where the control object is placed at the top right corner as compared to the bottom right corner. Furthermore, critical flow behavior is also dominant in that type of configuration, leading to increased fluid forces.

Conflict of Interest: Authors have no conflict of interest.

Data Availability Source: Data is confidential, but on demand of the Chief Editor or editor it can be provided on a reasonable matter.

Nomenclature:

C1	First object
C2	Second object
Cd_{mean}	Mean drag force
Cd_{rms}	Root mean square value of drag force
Cl_{rms}	Root mean square values of lift force
St	Strouhal number
Cd	Drag force
Cl	Lift force
d_1	Size of control object
d	Size of the main object
Re	Reynolds number
g_i	Distribution function
τ	Stability parameter
C_s	Speed of sound
L	Length of channel
H	Height of channel
Y_s	Vortex shedding frequency
U_{inf}	Uniform inflow velocity
w_i	Weighting coefficients

References:

[1] M. M. Zdravkovich, "The effect of interference between circular objects in cross flow," Strut, J. Fluids, vol. 1, pp. 239–261, 1987.

[2] K. Lam and W. C. Cheung, "Phenomena of vortex shedding and flow interference of three cylinders in different equilateral arrangements," J. Fluid Mech., vol. 196, pp. 1–26, Nov. 1988, doi: 10.1017/S0022112088002587.

[3] D. Sumner, S. J. Price, and M. P. Païdoussis, "Flow-pattern identification for two staggered circular cylinders in cross-flow," J. Fluid Mech., vol. 411, pp. 263–303, May 2000, doi: 10.1017/S0022112099008137.

[4] S. Balachandar and S. J. Parker, "Onset of vortex shedding in an inline and staggered array of rectangular cylinders," Phys. Fluids, vol. 14, no. 10, pp. 3714–3732, Oct. 2002, doi: 10.1063/1.1508101.

[5] M. H. Akbari and S. J. Price, "Numerical investigation of flow patterns for staggered cylinder pairs in cross-flow," J. Fluids Struct., vol. 20, no. 4, pp. 533–554, May 2005, doi: 10.1016/J.JFLUIDSTRUCTS.2005.02.005.

[6] O. Inoue, W. Iwakami, and N. Hatakeyama, "Aeolian tones radiated from flow past two square cylinders in a side-by-side arrangement," Phys. Fluids, vol. 18, no. 4, Apr. 2006, doi: 10.1063/1.2191847/915406.

[7] A. Agrawal, L. Djenidi, and R. A. Antonia, "Investigation of flow around a pair of side-by-side square cylinders using the lattice Boltzmann method," Comput. Fluids, vol. 35, no. 10, pp. 1093–1107, Dec. 2006, doi: 10.1016/J.COMPFLUID.2005.05.008.

[8] J. Niu and Z. Zhu, "Numerical study of three-dimensional flows around two identical square cylinders in staggered arrangements," Phys. Fluids, vol. 18, no. 4, Apr. 2006, doi: 10.1063/1.2194077/915470.

[9] B. S. Carmo and J. R. Meneghini, "Numerical investigation of the flow around two circular cylinders in tandem," J. Fluids Struct., vol. 22, no. 6–7, pp. 979–988, Aug. 2006, doi: 10.1016/J.JFLUIDSTRUCTS.2006.04.016.

[10] K. Lee and K. S. Yang, "Flow patterns past two circular cylinders in proximity," Comput. Fluids, vol. 38, no. 4, pp. 778–788, Apr. 2009, doi: 10.1016/J.COMPFLUID.2008.07.005.

[11] K. Fallah, A. Fardad, N. Sedaghatizadeh, E. Fattahi, and A. Ghaderi, "Numerical Simulation of Flow Around Two Rotating Circular Cylinders in Staggered Arrangement by Multi-Relaxation-Time Lattice Boltzmann Method at Low Reynolds Number," 2011.

[12] J. K. Ostanek and K. A. Thole, "Wake development in staggered short cylinder arrays within a channel," Exp. Fluids, vol. 53, no. 3, pp. 673–697, Sep. 2012, doi: 10.1007/S00348-012-1313-5/METRICS.

[13] R. Farzad, M., Amir, B. K., Ehsan, G & Mohammad, "Experimental Measurement of Turbulence Intensity of Flow Over Two object and Circular Object in Tandem Arrangement," 14th Eur. Turbul. Conf. Lyon, Fr., 2013.

[14] P. Anagnostopoulos and S. A. Seitanis, "Numerical study of aperiodic phenomena past two staggered rows of cylinders in cross-flow," Ocean Eng., vol. 92, pp. 212–233, Dec. 2014, doi: 10.1016/J.OCEANENG.2014.09.049.

[15] F. Tong, L. Cheng, and M. Zhao, "Numerical simulations of steady flow past two cylinders in staggered arrangements," J. Fluid Mech., vol. 765, pp. 114–149, Feb. 2015, doi: 10.1017/JFM.2014.708.

[16] D. Chatterjee and S. K. Gupta, "Convective Transport Around Rows of Square Cylinders Arranged in a Staggered Fashion at Moderate Reynolds Number," Numer. Heat Transf. Part A Appl., vol. 68, no. 4, pp. 388–410, Aug. 2015, doi:

10.1080/10407782.2014.986004.
[17] M. M. Alam, H. Bai, and Y. Zhou, "The wake of two staggered square cylinders," J. Fluid Mech., vol. 801, pp. 475–507, Aug. 2016, doi: 10.1017/JFM.2016.303.
[18] S. Yang, W. Yan, J. Wu, C. Tu, and D. Luo, "Numerical investigation of vortex suppression regions for three staggered circular cylinders," Eur. J. Mech. - B/Fluids, vol. 55, pp. 207–214, Jan. 2016, doi: 10.1016/J.EUROMECHFLU.2015.10.004.
[19] J. Aboueian and A. Sohankar, "Identification of flow regimes around two staggered square cylinders by a numerical study," Theor. Comput. Fluid Dyn., vol. 31, no. 3, pp. 295–315, Jun. 2017, doi: 10.1007/S00162-017-0424-2/METRICS.
[20] M. K. Chauhan, S. Dutta, B. S. More, and B. K. Gandhi, "Experimental investigation of flow over a square cylinder with an attached splitter plate at intermediate reynolds number," J. Fluids Struct., vol. 76, pp. 319–335, Jan. 2018, doi: 10.1016/J.JFLUIDSTRUCTS.2017.10.012.
[21] S. Fezai, F. Oueslati, and B. Ben-Beya, "Identification of flow states around three staggered square cylinders at two symmetrical arrangements by a numerical investigation," https://doi.org/10.1142/S012918312050151X, vol. 31, no. 11, Sep. 2020, doi: 10.1142/S012918312050151X.
[22] M. Raheela et al., "Numerical investigations for flow past two square rods in staggered arrangement through Lattice Boltzmann method," Ann. Math. Phys., pp. 016–027, Jul. 2021, doi: 10.17352/AMP.000021.
[23] M. Cheng, D. S. Whyte, and J. Lou, "Numerical simulation of flow around a square cylinder in uniform-shear flow," J. Fluids Struct., vol. 23, no. 2, pp. 207–226, Feb. 2007, doi: 10.1016/J.JFLUIDSTRUCTS.2006.08.011.
[24] D. T. Sukop, M. C. & Thorne, "Lattice Boltzmann modeling: an introduction for scientists and Engineers," Springer Berlin Heidelb., 2005.
[25] D. Yu, R. Mei, L. S. Luo, and W. Shyy, "Viscous flow computations with the method of lattice Boltzmann equation," Prog. Aerosp. Sci., vol. 39, no. 5, pp. 329–367, Jul. 2003, doi: 10.1016/S0376-0421(03)00003-4.
[26] A. A. Mohammad, "Lattice Boltzmann Method: Fundamentals and Engineering Applications with Computer Codes," Springer, 2011.
[27] D. A. Wolf-Gladrow, "Lattice-gas cellular automata," pp. 39–138, 2000, doi: 10.1007/978-3-540-46586-7_3.
[28] S. Chen and G. D. Doolen, "Lattice boltzmann method for fluid flows," Annu. Rev. Fluid Mech., vol. 30, no. Volume 30, 1998, pp. 329–364, Jan. 1998, doi: 10.1146/ANNUREV.FLUID.30.1.329/CITE/REFWORKS.
[29] "Lattice Boltzmann Method: Fundamentals and Engineering Applications with Computer Codes | SpringerLink." Accessed: Apr. 19, 2024. [Online]. Available: https://link.springer.com/book/10.1007/978-0-85729-455-5
[30] "Low-Reynolds-number flow around a square cylinder at incidence: study of blockage, onset of vortex shedding and outlet boundary condition - Sohankar - 1998 - International Journal for Numerical Methods in Fluids - Wiley Online Library." Accessed: Apr. 19, 2024. [Online]. Available: https://onlinelibrary.wiley.com/doi/abs/10.1002/%28SICI%291097-0363%2819980115%2926%3A1%3C39%3A%3AAID-FLD623%3E3.0.CO%3B2-P
[31] "CFD ANALYSIS OF 2D UNSTEADY FLOW AROUND A SQUARE CYLINDER." Accessed: Apr. 19, 2024. [Online]. Available: https://www.researchgate.net/publication/331563254_CFD_ANALYSIS_OF_2D_UNSTEADY_FLOW_AROUND_A_SQUARE_CYLINDER
[32] G. R. Vamsee, M. L. De Tena, and S. Tiwari, "Effect of arrangement of inline splitter

plate on flow past square cylinder," Prog. Comput. Fluid Dyn., vol. 14, no. 5, pp. 277–294, 2014, doi: 10.1504/PCFD.2014.064554.

[33] "Large eddy simulation of the subcritical flow past a circular cylinder: numerical and modeling aspects - Breuer - 1998 - International Journal for Numerical Methods in Fluids - Wiley Online Library." Accessed: Apr. 19, 2024. [Online]. Available: https://onlinelibrary.wiley.com/doi/abs/10.1002/%28SICI%291097-0363%2819981215%2928%3A9%3C1281%3A%3AAID-FLD759%3E3.0.CO%3B2-%23

[34] A. Okajima, "Strouhal numbers of rectangular cylinders," J. Fluid Mech., vol. 123, pp. 379–398, 1982, doi: 10.1017/S0022112082003115.